Available online at www.sciencedirect.com
SCIENCE DIRECT®
Geochimica et Cosmochimica Acta 70 (2006) 118–132
Geochimica
www.elsevier.com/locate/gca

Iron isotopes in natural carbonate minerals determined by MC-ICP-MS with a ^{58}Fe–^{54}Fe double spike

K. Dideriksen [a,*], J.A. Baker [b,c], S.L.S. Stipp [a]

[a] Geological Institute, University of Copenhagen, Øster Voldgade 10, DK-1350 Copenhagen, Denmark
[b] Danish Lithosphere Centre, Øster Voldgade 10, DK-1350 Copenhagen, Denmark
[c] School of Earth Sciences, Victoria University of Wellington, P.O. Box 600 Wellington, New Zealand

Received 3 December 2004; accepted in revised form 25 August 2005

Abstract

We have developed a method for iron isotope analysis by multiple-collector inductively coupled plasma mass spectrometry (MC-ICP-MS) using a ^{58}Fe–^{54}Fe double spike. A 20 min analysis produces mass-bias-corrected iron isotope data with an external reproducibility of ±0.05‰ (2 SD) on $\delta^{56}Fe$, which represents a decrease in analysis time compared to sample-standard bracketing techniques. The estimation of external reproducibility is based on replicate analysis of the ETH hematite in-house standard. The double spike method has two advantages. First, matrix effects during MC-ICP-MS analysis are decreased with tests showing that accurate iron isotope data can, in some cases, be obtained even when matrix levels exceed iron concentration (Na/Fe, Mg/Fe, and Ca/Fe up to 5, 2, and 0.1, respectively). Because chemical separation reduces matrix/Fe to levels more than three orders of magnitude lower than this, measured Fe isotope compositions are unlikely to be compromised by matrix effects. Second, it is possible to spike samples before chemical purification, which enables any isotopic fractionation effect because of incomplete recovery of iron from a sample to be accounted for. This may be important where obtaining quantitative iron yields from samples is difficult, such as the extraction of dissolved iron from water samples. Fe isotope data on a set of standard reference materials (igneous rocks, ferromanganese nodules, sedimentary rocks, and ores) are presented, which are in agreement with previously published data considering analytical uncertainties. Mantle-derived standard rock samples that are the source of iron for surficial, (bio)geochemical cycling yield a mean $\delta^{56}Fe$ of 0.041 ± 0.11‰ ($n = 8$; 2 SD) with reference to IRMM-14. Hydrothermal and metamorphic calcium carbonate rocks with a relatively low iron content (100–4000 ppm) have $\delta^{56}Fe = -1.25$ to -0.07‰. Structural Fe(II) in hydrothermal calcites has $\delta^{56}Fe = -1.25$ to -0.27‰. The light iron in this range of carbonate minerals may reflect the iron isotope composition of the hydrothermal fluids from which the carbonate precipitated, or the presence of Fe(III) and/or organic material in the hydrothermal fluids during calcite precipitation.

1. Introduction

Four stable isotopes of iron exist—^{54}Fe, ^{56}Fe, ^{57}Fe, and ^{58}Fe—which may undergo mass-dependent fractionation during physical, chemical, and biological processes in a manner similar to that observed for stable isotopes of lighter elements such as H, C, and O. However, compared to these light elements, which are predominantly covalently bonded in nature, isotopic variations of natural Fe are significantly smaller (e.g., Beard and Johnson, 1999; Beard et al., 2003a). Mantle-derived rocks, the parent material for (bio)geochemical cycling, appear to be largely homogeneous with respect to Fe isotopes with values quoted for $\delta^{56}Fe = 0.068 \pm 0.08$‰ ($n = 13$; 2 standard deviations (SD); Poitrasson et al., 2004) and $\delta^{56}Fe = 0.09 \pm 0.10$‰ ($n = 46$; 2 SD; Beard et al., 2003a) (with respect to the IRMM-14 Fe standard). For mantle spinels, however, variable Fe isotope compositions have been determined that correlate with Fe oxidation state (Williams et al., 2004). Larger Fe isotope fractionation has been observed for material formed at lower temperatures. For example, marine ferromanganese crusts and nodules are isotopically

* Corresponding author.
E-mail addresses: knudd@geol.ku.dk (K. Dideriksen), stipp@geol.ku.dk (S.L.S. Stipp).

0016-7037/$ - see front matter © 2005 Elsevier Inc. All rights reserved.
doi:10.1016/j.gca.2005.08.019

lighter than igneous material by up to 0.8‰ (Beard et al., 1999; Levasseur et al., 2004; Zhu et al., 2000) and fluids from hydrothermal vents close to oceanic spreading ridges are also characterised by isotopically light Fe (Beard et al., 2003b; Severmann et al., 2004; Sharma et al., 2001). Isotopic fractionation of iron observed in nature and in the laboratory has been attributed to abiotic processes (Anbar et al., 2000; Bullen et al., 2001), including redox reactions (Johnson et al., 2002), as well as biotic processes, such as dissimilatory Fe reduction (Beard et al., 1999). Indeed, human blood constitutes the most fractionated natural material analysed so far (Walczyk and von Blanckenburg, 2002; Zhu et al., 2002).

The first relatively precise Fe isotope analyses of natural materials were made by thermal ionisation mass spectrometry (TIMS) using a ^{58}Fe–^{54}Fe double spike to correct for instrumental mass fractionation (Johnson and Beard, 1999), but the recent development of multiple-collector inductively coupled plasma mass spectrometers (MC-ICP-MS) has facilitated a rapid increase in Fe isotope studies. However, the use of MC-ICP-MS for Fe isotope studies is not straightforward. First, during plasma ionisation, argide molecular species, such as $^{40}Ar^{14}N^+$, $^{40}Ar^{16}O^+$, and $^{40}Ar^{16}OH^+$, are produced that constitute significant isobaric interferences on ^{54}Fe, ^{56}Fe, and ^{57}Fe. ^{58}Ni released from the Ni-coated sample and skimmer cones during analysis also forms a minor background interference, although aluminium or platinum cones may be used to circumvent this. Most first- and second-generation MC-ICP-MS instruments lack the mass resolution to allow separation of these isobaric interferences from the Fe signal, while providing the well-defined, flat-topped peaks that are required for precise isotope ratio determinations. The second complication is the need to correct for instrumental mass bias that occurs during analysis. The mass bias that affects the Fe isotope analysis using MC-ICP-MS is of the order of 40‰ per atomic mass unit (amu) and >10 times larger than natural isotopic variations observed to date. Reliable correction for this instrumental mass bias is vital for producing both precise and accurate Fe isotope data.

To date, measurement of Fe isotope ratios by MC-ICP-MS has relied on sample-standard bracketing or external normalisation techniques (e.g., Sharma et al., 2001; Zhu et al., 2000). For sample-standard bracketing, it is assumed that the instrumental mass bias is identical during standard and sample analysis. Unfortunately, this method requires frequent measurement of bracketing standards because of unstable source conditions and, typically, each individual sample must be measured multiple times. Samples are usually measured 3–6 times with corresponding 4–7 measurements of the standard (e.g., Poitrasson et al., 2004), so each sample analysis represents the combined result of 7–13 separate measurements. This represents 1–2 h of instrument time, given that each measurement takes 10 min including washouts, background measurements, and sample uptake. Importantly, the instrumental mass bias is affected by the presence of matrix impurities (typically referred to as the ''matrix effect'') and differences in Fe oxidation states (Zhu et al., 2002), so samples must be treated to remove matrix elements prior to analysis.

An alternative method to correct for instrumental mass bias is the external normalisation method where the mass bias of Cu or Ni isotopes is used to account for the instrumental mass bias of Fe isotope ratios during measurement (e.g., Kehm et al., 2003; Malinovsky et al., 2003; Sharma et al., 2001). The relative mass bias of Fe, Cu, and Ni isotopes varies with instrument performance, but for intervals of several hours values are related, providing a basis for correcting measured Fe isotope ratios. The precision of this method relies on identification of the correlation that characterises the mass biases of Fe and Cu or Ni isotopes through analysis of doped standards that bracket the analysis of samples. In practice, it requires almost as many analyses as the conventional sample-standard bracketing technique. Although the external normalisation method seems less susceptible to matrix artefacts than sample-standard bracketing (Arnold et al., 2004), other studies have suggested that the mass bias of isotopes of different elements is affected variably by matrix impurities (Ingle et al., 2003), meaning that the external normalisation method may also, to some extent, be compromised by matrix effects. In addition, for some instruments, the use of Cu-doping requires an extra measurement cycle because the collector arrays cannot simultaneously monitor masses 54 to 65 (Roe et al., 2003).

Notwithstanding these difficulties, most MC-ICP-MS Fe isotope studies have achieved an external reproducibility equivalent to ±0.1‰ (2 SD) for the δ^{56}Fe, permitting resolution of significant Fe isotope variations in natural materials. However, this external reproducibility is considerably larger than the internal precision typically obtainable on the ^{56}Fe/^{54}Fe ratio (2 standard error (SE) < ±0.02‰; 2 SE = 2 SD/$\sqrt{n}$) for a single isotope analysis, even though the final result often represents an average of several such measurements. Presumably, matrix effects and fluctuating instrumental mass bias degrade the final external reproducibility of sample analyses. Correction for isobaric interferences may also contribute to uncertainties.

Given the time-consuming nature of sample-standard bracketing methods for Fe isotope analysis and apparent limitations on data reproducibility, we have chosen to explore the potential of Fe isotope analysis by MC-ICP-MS using a Fe double spike (DS) to correct for instrumental mass bias. The double (or triple) spike method is well established as a robust approach for correction of instrumental mass bias during mass spectrometric measurement of isotope ratios (e.g., Hofmann, 1971) and, indeed, the first precise Fe isotope data for natural materials obtained by TIMS employed this approach (Johnson and Beard, 1999). DS-methods have several advantages over other MC-ICP-MS methods for Fe isotope analysis: (1) natural mass-dependent fractionation of Fe may be resolved in one analysis, so time-consuming analysis of a larger num-

ber of standards than samples is avoided; (2) variations in plasma-source conditions, matrix effects (within reasonable limits!), and Fe oxidation states should not affect the DS-analysis; (3) the relative contribution of isobaric interferences on the spiked isotopes is significantly reduced; and (4) samples may be spiked before chemical purification, so that any isotope fractionation that might occur during sample preparation is, in principle, accounted for.

Herein, we describe a rapid method for Fe isotope ratio measurement with a ^{58}Fe–^{54}Fe DS using a double focusing MC-ICP-MS. The robustness of the method is demonstrated by studying the effects of matrix elements on the analytical results. The matrices investigated consisted of Na and Mg, which are believed to modify instrumental mass bias through the ''space-charge'' effect (Douglas and Tanner, 1998) and Ca, whose polyatomic nitride, oxide, and hydroxide species are isobaric with ^{54}Fe, ^{56}Fe, and ^{57}Fe. Our DS-method is capable of yielding precise Fe isotope data (±0.05‰, 2 SD, $\delta^{56}Fe$) with a single analysis and the analysis is unaffected by the presence of significant amounts of matrix elements even at ratios of Na/Fe $\leqslant$ 5, Mg/Fe $\leqslant$ 2, and Ca/Fe $\leqslant$ 0.1. We present Fe isotope results for a set of international standard reference materials and on a suite of calcium carbonate minerals formed under various geological conditions. These results are among the first Fe isotope data reported for low-Fe carbonates (100–4000 ppm) and show significant variations. Hydrothermal calcite has light Fe, which is either inherited from the isotope composition of the hydrothermal solutions from which it precipitated, or reflects the presence of aqueous Fe(III)– or Fe(II)–organic complexes that fractionated the Fe isotopes at the time of Fe(II) incorporation into the calcite structure.

2. Standard materials and geological samples

All standard reference materials and samples are listed and described in Tables 1 and 2. The Fe isotope reference standard (IRMM-14) was used as the reference standard for this study (Institute of Reference Material and Measurement, Geel, Belgium). A set of international standard reference materials, encompassing a range of geological matrices, were obtained from the United States Geological Survey (USGS) and the National Institute of Standards and Technology (NIST). In addition, a Type IIIAB iron meteorite (Cape York) and a hematite in-house standard from ETH-Zürich were also analysed.

The natural calcium carbonate samples were acquired from the geological museums of Copenhagen and Oslo, and represent various formation conditions including magmatic, hydrothermal, and metamorphic carbonates (Table 2). Samples of limestone and highly crystalline calcites were also collected from a $500 \times 500 \times 100$ m^3 part of the Steinvika Formation (Norway), where a felsic igneous intrusion triggered hydrothermal recrystallisation of Ordovician limestone in fluid-bearing fractures. All samples were shown by XRD (X-ray diffraction) to be pure calcite (2% detection limit) except one, which had a very small amount of quartz. AAS (atomic absorption spectroscopy) showed concentrations of Mg, Mn, and Fe to be in the range of a few to several hundred ppm (Harstad, personal communication). One sample was banded with visible differences in colour. Fe and Mn in the two regions were ca. 4000 ppm. To investigate Fe bonding character, subsamples from the two parts of the sample were analysed with Mössbauer spectroscopy (MS). The transparent, colourless region showed MS absorption lines typical for Fe substituted in the Ca sites in calcite, whereas material

Table 1
Standard reference materials and other analysed standards

Sample	Description	Fe (wt%)[a]
USGS standards		
AGV-2	Andesite from Guano Valley, Lake County, Oregon	4.7
BCR-2	Columbia River basalt sampled near Portland, Oregon	9.7
BHVO-2	Hawaiian Volcanic Observatory basalt	8.6
BIR-1	Coarse-grained, olivine tholeiitic basalt from Iceland	7.9
COQ-1	Carbonatite from Oka Complex, Lake Two Mountains, Montreal	2.0
CLB-1	Bituminous coal from Lower Bakerstown coal bed	0.9
DNC-1	Olivine-normative dolerite from Braggstown, North Carolina	6.9
DTS-2	Dunite from Twin Sisters Mountain Range, Bellingham, Washington	5.4
GSP-2	Granodiorite from Silver Plume, Colorado	3.4
NOD-A-1	Ferromanganese nodule from the Atlantic Ocean, Blake Plateau, 31°02′N, 78°22′W (788 m depth)	10.9
NOD-P-1	Ferromanganese nodule from the Pacific Ocean, 14°50′N, 124°28′W (4300 m depth)	5.8
MAG-1	Clayish sediment with low carbonate content from Wilkinson Basin, Gulf of Maine, 125 km east of Boston	4.8
SGR-1	Shale from the Mahogany zone, Green River Formation	2.1
NIST standards		
SRM-692	Iron ore from Labrador, Canada	59.6
SRM-8455	Pyrite ore from New Mexico	—
Other standards		
Cape York	Type IIIAB iron meteorite	—
ETH-Hematite	Hematite in-house standard from ETH-Zürich	—

[a] Data from USGS (http://minerals.cr.usgs.gov/geo_chem_stand/) and NIST (http://ts.nist.gov/ts/htdocs/230/232/232.htm).

Table 2
Natural calcium carbonate samples

Environment	Sample	Origin	Notes
Magmatic	MAG BB 10	Grønnedal, Ikka, Greenland	
Skarn	S-89a	Gråttådalen, Beiarn, Norway	
Marble	LS 9	Amdrup Land, Greenland	
Limestone	SLS 08	Steinvika Formation, Norway	
	SLS 10	Steinvika Formation, Norway	
	L BB3	Närke, Sweden	
Hydrothermal	HT/RM 326	Sigdal, Norway	
	HT 9572	Chihuahua, Mexico	
	HT 9426	Himmelfürst, Freiburg, Germany	
Calcites	HTC 4	Steinvika Formation, Norway	
	HTC 12	Steinvika Formation, Norway	
	HTC 28	Steinvika Formation, Norway	Contains traces of quartz
	HTC 38	Steinvika Formation, Norway	Fe dominantly in goethite
	HTC 40	Steinvika Formation, Norway	Fe only in calcite
Pegmatite	P 31867	Averøya Vevang, Møreog Romsdal, Norway	
	P 9710	Nedre Salbutangen, Krageø, Norway	
Slickenslide	Slick 1	New Zealand	Calcite slickenslide in Tertiary fault zone cutting greywacke-argillite sediments

from the brownish, cloudy region also produced lines indicating that goethite hosted 80% of the Fe. The two subsamples were analysed separately for Fe isotopes. In addition to the Steinvika hydrothermal samples, calcites from other lithologies, including metamorphic skarn and marble, sedimentary limestone, igneous pegmatite, and a slickenside from a Tertiary fault cutting greywacke, were also analysed.

3. Methods

3.1. Sample preparation and chemical separation of iron

Sample preparation was carried out using ultrapure, quartz sub-boil distilled, HCl, and HNO_3, and Milli-Q water with a resistivity of $>18\ M\Omega$. Teflonware used in sample preparation was cleaned by sequential immersion in analytical grade 7 M HNO_3 and 6 M HCl at 90 °C, followed by exposure to ultrapure 6 M HCl at 140 °C. The few Teflon beakers that had been in contact with the DS were additionally washed three times with ultrapure 6 M HCl to minimise potential problems with sample memory. Chemical separation of Fe was performed using anion exchange resin in chloride form (Bio-Rad AG-1 X4, 200–400 mesh). Procedural blanks contained $\leqslant 5$ ng of Fe, an insignificant amount for this study.

Silicate samples were digested in a mixture of 40% HF and concentrated HNO_3, whereas metal, iron oxyhydroxide, and calcium carbonate samples were dissolved in 6 M HCl. The coal sample was first cindered to ash and then dissolved in a mixture of 40% HF and concentrated HNO_3 acid. One silicate-bearing limestone (SLS 10) was also partially digested in 6 M HCl to test for potential isotopic fractionation effects during dissolution. All samples were digested in sealed Savillex Teflon beakers for 24 h at 140 °C. After initial dissolution, selected samples were spiked, referred to hereafter as prespiked. All the samples were then evaporated to dryness and put through two concentrated HNO_3 dissolution/evaporation steps to oxidise the Fe and organic material. The nitrate content of the samples was subsequently reduced through evaporation of 6 M HCl. After redissolution in 6 M HCl, the HCl digested nodule samples and SLS-10 that had undissolved material were centrifuged to separate the solid from the solution.

Aliquots of solutions were then passed through anion exchange columns to yield about 40–100 μg Fe. All natural samples and standard reference materials, as well as some IRMM-14 standards, were chemically purified using procedures similar to those described by Levasseur et al. (2004). These authors evaluated the robustness of their procedure and found that: (1) the Fe yield was 100% (±3%), (2) several purification passes of pure Fe standards did not affect the measured Fe isotope composition, and (3) the measured isotope composition of IRMM-14 separated from synthetic mixtures of IRMM-14 and the Fe-free matrix of selected samples yielded the IRMM-reference value. Briefly, in our study the samples were loaded onto columns constructed from 1 mL polypropylene pipette-tips containing 0.5 mL of anion exchange resin. Matrix elements were eluted with 6 reservoirs of 1 mL of 6 M HCl and Fe was subsequently collected in 4 reservoirs of 1 mL of 0.05 M HCl. Samples with low Fe content were subjected to more than one chemical separation pass to minimise possible matrix interferences. Each pass was preceded by a HNO_3 evaporation step to oxidise Fe. After chemical separation and evaporation of the collected Fe, chloride concentration was minimised through two HNO_3 dissolution/evaporation steps. The samples were then dissolved in 2% HNO_3 and their Fe concentration was determined semi-quantitatively. A fraction of the sample solution contain-

ing ca. 20 μg natural Fe was then transferred to a 2 mL disposable centrifuge tube and diluted to 20 ppm, after which the unspiked samples were spiked with the DS.

Most of the samples were spiked after purification for the following reasons: (1) All studies of similar Fe purification procedures have shown the anion exchange chromatography to be robust with yields that are essentially quantitative (Arnold et al., 2004; Brantley et al., 2004; Dauphas et al., 2004; Kehm et al., 2003; Levasseur et al., 2004; Matthews et al., 2004; Poitrasson et al., 2004; Rouxel et al., 2003; Sharma et al., 2001; Williams et al., 2004; Zhu et al., 2002). (2) Unnecessary consumption of the expensive DS could be minimised because only the fraction of the purified sample that was analysed required spiking. (3) Fe concentrations need not be known accurately before sample processing. High-precision determination of Fe isotope composition by DS methods requires a relatively close matching of spike and natural Fe concentrations, which is easier to achieve after sample processing.

Given that matrix elements present in samples may not always be removed during chemical separation and incomplete dissolution or the presence of Fe complexes could compromise the results, a number of experiments were performed to validate the analytical protocols: (1) To test the matrix sensitivity of DS analysis of Fe isotope ratios, IRMM-14 standards were doped with varying amounts of Na, Mg, and Ca, and analysed without purification. (2) To test that matrix elements, which have isobaric interferences with Fe, were adequately removed from solution during chemical purification, samples of IRMM-14 doped with large quantities of Ca, Cr, and Ni were subjected to our anion exchange separation procedures and the collected Fe was analysed. (3) To test that fractionation was not prone to occur during HCl dissolution of the carbonate and Fe-oxyhydroxide samples because of partial digestion, the organic-containing, silicate-bearing limestone (SLS-10), that after HCl digestion contained the most residual material of all processed samples, was also subjected to HF dissolution. (4) To test that organically complexed Fe was not prone to fractionation during sample processing, the solution from the HCl digestion of SLS-10 was centrifuged and separated into two equal portions. One part was treated "normally," while the other part was spiked, exposed to two HNO_3 evaporation steps and one HCl evaporation step before dissolution in 6 M HCl and chemical purification. Finally, a pure IRMM-14 sample and an IRMM-14 sample that had been doped with the Fe-complexing ligand, citrate, were also passed through chemical separation and analysed.

3.2. Iron double spike

^{54}Fe and ^{58}Fe spikes were purchased from the Oak Ridge National Laboratory. The DS procedure has been used to correct for instrumental mass bias of numerous isotope systems including Pb, Fe, and Mo, and researchers have adopted various mathematical approaches to deconvolve the mass-fractionation-corrected isotope ratios (e.g., Eugster et al., 1969; Hofmann, 1971; Johnson and Beard, 1999; Siebert et al., 2001). In this work, we use the iterative approach of Siebert et al. (2001), developed for Mo isotope analysis by MC-ICP-MS. In that study, the authors assumed that both natural and instrumental mass-dependent fractionation follow an exponential law. However, in the data reduction, the exponential geometry is iteratively approximated linearly. The exponential law has previously been shown to be a good approximation for instrumental mass-dependent fractionation for several isotope systems (e.g., Zn; Maréchal et al., 1999), including Fe isotopes, during MC-ICP-MS analysis (Arnold et al., 2004). Because all natural isotopic variations in terrestrial material can be anticipated to lie on the mass-dependent fractionation curve, only a single (spiked) analysis is necessary to determine the true Fe isotope composition.

The exact composition of the DS and also the sample to spike ratio must be considered during DS analysis in order to minimise error magnification during data acquisition and reduction. For Fe isotopes, calculations for a range of double and triple spike compositions show that a DS composed of ~90% ^{54}Fe and ~10% ^{58}Fe leads to minimum error magnification for spike/sample ratios ranging from 0.6 to 9 (Johnson and Beard, 1999; our calculations). In this study, a DS composed of ~93% ^{54}Fe and ~7% ^{58}Fe was used to provide $^{54}Fe/^{56}Fe \sim 1$ in sample-spike mixtures. Several calibrations of the DS using IRMM-14 as the standard yielded the following composition: $^{54}Fe/^{56}Fe = 27.76 \pm 0.03$; $^{57}Fe/^{56}Fe = 0.05495 \pm 0.00006$; $^{58}Fe/^{56}Fe = 2.044 \pm 0.003$ (2 SD).

3.3. Mass spectrometry

Fe isotope analysis was carried out on a double focusing Thermoelemental AXIOM MC-ICP-MS. Samples were introduced with a CETAC Aridus desolvating nebuliser using only argon as a sweep gas. Static measurement of the Fe isotope masses was conducted using a Faraday collector array equipped with 10^{11} Ω resistors (Table 3). Mass 53 was also monitored for isobaric interferences of Cr on mass 54. Based on a natural $^{54}Cr/^{53}Cr$ ratio of 0.2495, the contribution of ^{54}Cr to the ^{54}Fe signal never exceeded 0.005‰ during analysis. Using MC-ICP-MS, each sample was screened prior to analysis to ensure it did not contain detectable amounts of Ni.

During Fe isotope analytical sessions, the sensitivity of the mass spectrometer was decreased by closing the collector slits, so that 2 ppm Fe approximately represented 1 V signal. The use of higher Fe loading reduces the relative magnitude of isobaric interferences of ArN^+, ArO^+, and $ArOH^+$, as well as ^{58}Ni emanating from the skimmer cones. Any remaining interferences were corrected for by using on-peak-zero (OPZ) procedures while aspirating the 2% HNO_3 used to dissolve samples and standards. An

Table 3
Faraday collector array used to measure Fe isotopes with main interfering species

Collector	L4	L2	H1	H2	H4
Mass	53	54	56	57	58
Fe isotope	—	^{54}Fe	^{56}Fe	^{57}Fe	^{58}Fe
Interferences	^{53}Cr	^{54}Cr	—	—	^{58}Ni
		^{40}Ar^{14}N	^{40}Ar^{16}O	^{40}Ar^{16}OH	
		^{40}Ca^{14}N	^{40}Ca^{16}O	^{40}Ca^{16}OH	

Table 4
Typical ion beam intensities measured during sample and on-peak zero analysis

Mass	Sample signal (V)	Typical blank signal and range (mV)	Contribution to sample signal (‰)
54	8	0.5 (0.55–0.45)	0.07
56	8	0.4 (0.45–0.35)	0.06
57	0.20	0.01 (0.015–0.005)	0.05
58	0.65	0.05 (0.06–0.04)	0.07

entire analytical cycle consists of ca. 5–10 min of washout with 2% HNO_3, 5 min of OPZ measurement, and 14 min of sample measurement. All data were acquired in four blocks using either 40 (OPZ measurements) or 100 (sample measurements) two-second integrations. Baseline measurements were made at half-masses for 30 s prior to each analytical block so that the exact isotope composition of the memory could be monitored in the OPZ analysis. Solution concentrations were typically 20 ppm and with an uptake rate of 60 μL/min, each analysis consumes about 20 μg of Fe.

Table 4 shows the typical ion beam intensities during sample analysis and, more importantly, the intensity range of isobaric interferences during OPZ measurements. It is apparent that the careful determination of the very small, fluctuating, $ArOH^+$ interference on mass ^{57}Fe is critical for precision when using DS methods, because ^{57}Fe concentration is so low in the spiked samples. Also, the uncertainties on the ^{57}Fe/^{56}Fe ratio propagate by a factor >2 onto the ^{56}Fe/^{54}Fe ratio during data reduction. While a ^{57}Fe-containing triple spike might mitigate this problem by increasing the signal on mass 57, such a triple spike composition has an unfavourably large error magnification during data reduction (Johnson and Beard, 1999).

3.4. Data reduction

The first step of data reduction is correction for argide interferences through subtraction of the OPZ signals from the Fe signals. The mean OPZ measurement from *before and after* each analysis is used to make the correction, and constancy of OPZ measurements before and after analysis can be used to assess the integrity of the analysis. At no point were the OPZ measurements found to drift. However, difficulty in measuring the intensity of the very small background on mass 57 meant that approximately 2% of our isotope analyses were discarded because the two OPZ corrections introduced a > 0.04‰ difference in the corrected ^{57}Fe/^{56}Fe ratios. Corrected ^{54}Fe/^{56}Fe, ^{57}Fe/^{56}Fe, and ^{58}Fe/^{56}Fe ratios are then entered into an Excel spreadsheet, where the iterative DS data reduction of Siebert et al. (2001) is used to devolve the mass-bias-corrected Fe isotope ratios based on the calculation of a single fractionation factor which is applied to all ratios.

The error propagation that occurs during data reduction and the difficulty in measuring the ^{57}Fe/^{56}Fe ratio means that the internal precision of mass-bias-corrected Fe isotope ratios is closely linked to the internal precision of the measurement of this ratio. Given typical internal errors for ^{57}Fe/^{56}Fe of 0.022–0.028‰ (2 SE), the typical internal precision for mass-bias-corrected ^{56}Fe/^{54}Fe is ca. 0.06‰ (2 SE).

All Fe isotope ratios in this study are reported relative to IRMM-14 in the per mil notation (‰)

$$\delta^{56}\mathrm{Fe} = \left(\frac{(^{56}\mathrm{Fe}/^{54}\mathrm{Fe})_{\mathrm{sample}}}{(^{56}\mathrm{Fe}/^{54}\mathrm{Fe})_{\mathrm{IRMM\text{-}14}}} - 1 \right) \times 10^3.$$

4. Results

4.1. Analysis of the IRMM-14 and the ETH in-house standards

Replicate measurements of IRMM-14 standards within individual sessions yield a reproducibility of ±0.05 to 0.07‰ for the ^{56}Fe/^{54}Fe ratio (2 SD; $n \geqslant 7$), which is comparable to the calculated internal precision (2 SE) of the individual analyses after errors have been propagated through the DS-correction. Except for internal precision of analyses, which are given as 2 SE, all uncertainties are quoted at the 2 SD level. From session-to-session, however, the mean values defined by replicate analysis of IRMM-14 vary slightly more, by a maximum of 0.2‰ (Fig. 1). To account for these effects, the average of replicate analyses of the IRMM-14 standard during each session is used to make a small secondary correction to normalise the data for the natural samples. Our reproducibility for the IRMM-14 standard measurements within individual sessions is also comparable to the external reproducibility obtained on repeated analyses of an ETH in-house hematite standard

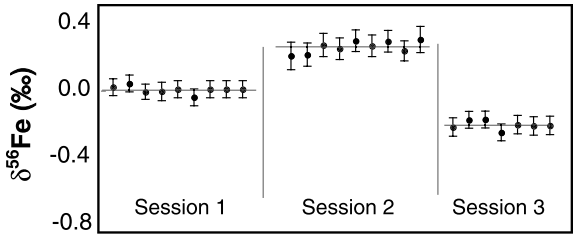

Fig. 1. Fe isotope results for IRMM-14 standards collected during three separate analytical sessions. The mean value for each session (represented by the horizontal lines) is used to make a small secondary normalisation to the results for natural samples.

Table 5
DS-corrected Fe isotope ratios of IRMM-14 samples with variable $^{54}Fe/^{56}Fe$ ratios after spiking and doped with Na, Mg or Ca

Type	IRMM-14	$\delta^{56}Fe$ (‰)	2 SE[a]
Variable sample:spike	$^{54}Fe/^{56}Fe \sim 0.6$	−0.07	0.07
	$^{54}Fe/^{56}Fe \sim 1.5$	−0.05	0.10
Na added	Na/Fe = 0.02	0.05	0.07
	Na/Fe = 0.2	0.02	0.06
	Na/Fe = 2	0.02	0.06
	Na/Fe = 5	−0.01	0.05
	Na/Fe = 20	−0.07	0.06
Mg added	Mg/Fe = 0.02	0.00	0.06
	Mg/Fe = 0.2	−0.02	0.06
	Mg/Fe = 2	−0.06	0.05
	Mg/Fe = 5	−0.10	0.06
Ca added	Ca/Fe = 0.005	−0.04	0.06
	Ca/Fe = 0.005	−0.01	0.06
	Ca/Fe = 0.04	−0.04	0.06
	Ca/Fe = 0.1	−0.01	0.06
	Ca/Fe = 0.3	0.14	0.06
	Ca/Fe = 1.5	0.42	0.07

[a] Propagated internal precision of each analysis.

performed over a six-month period ($\delta^{56}Fe = 0.58 \pm 0.05$‰; $n = 8$). The determined Fe isotope composition for this hematite standard is in excellent agreement with results obtained at ETH, Zürich ($\delta^{56}Fe = 0.58 \pm 0.09$‰; $n = 250$; Williams et al., 2004).

All of our analysed standard reference materials and samples were spiked so the $^{54}Fe/^{56}Fe$ ratio was within the range of 0.8–1.2. However, we also analysed IRMM-14 with different spike to sample ratios ($^{54}Fe/^{56}Fe$ ratios of 0.6 and 1.5). Within the internal precision of the measurements, the determined Fe isotope compositions were identical to the IRMM-14 reference value (Table 5), indicating that variations in spiking ratios and potential instrument memory effects do not affect the analytical results. Also, results for IRMM-14 standards analysed just after samples having $^{54}Fe/^{56}Fe$ ratios close to 0.8 or 1.2 do not differ significantly or systematically from the mean IRMM value. If memory effects did indeed compromise the results, one would see an effect on these samples.

4.2. Results of tests to evaluate isobaric interferences and matrix influence

The presence of matrix elements in the plasma source may compromise the determination of Fe isotopes by production of isobaric interferences and also by affecting the charge density of the ion flow, changing the instrumental mass bias through the "space-charge" effect (Douglas and Tanner, 1998). For determination of Fe isotope ratios by the DS method, correction of argide and ^{58}Ni isobaric interferences is critical. The reproducibility of the ETH in-house standard measurements is comparable to the internal precision of the analyses, suggesting that the OPZ background measurement adequately deals with these interferences. While the measured OPZ in 2% HNO_3 may not mimic completely the interferences that occur during the Fe isotope measurement because of matrix effects caused by Fe, normalisation of results to those of IRMM-14, which had similar analyte loading, accounts for this effect.

Unlike Ar-based and Ni interferences, ions left after sample purification cannot be corrected for by OPZ. The effects on DS-corrected Fe isotope ratios of adding variable amounts of the common elements Na, Mg, and Ca to IRMM-14 were investigated (Figs. 2 and 3; Table 5). No significant Fe signal suppression effects (i.e., >20%) were observed from the addition of large amounts of matrix elements. Results obtained for Na and Mg doping experiments in two different sessions show that high concentrations of these matrix elements, even at levels that can exceed the Fe concentration (Na/Fe $\leqslant$ 5; Mg/Fe $\leqslant$ 2), do not significantly affect the DS-corrected Fe isotope ratios determined on IRMM-14. These results contrast with those for similar experiments where the instrumental mass bias was corrected using standard-sample bracketing (Albarède and Beard, 2004). Here, analysis of Fe isotope compositions was compromised at much lower matrix to Fe ratios (Fig. 2).

Ca forms $^{40}CaN^+$, $^{40}CaO^+$, and $^{40}CaOH^+$ species during analysis that are isobaric with ^{54}Fe, ^{56}Fe, and ^{57}Fe. Clearly, Ca is present in very large amounts in the calcium carbonate samples (Ca/Fe > 200) so residual Ca may be present in samples after anion exchange leading to erroneous results. For example, for cold plasma analysis, $^{40}CaOH^+/Ca^+$ may be as large as 0.2, impairing meaningful measurement of ^{57}Fe (Kehm et al., 2003). To probe the effect of polyatomic Ca interferences on DS Fe isotope measurements, IRMM-14 samples were doped with various amounts of Ca and analysed. The results show that Ca-based interferences lead to erroneous positive $\delta^{56}Fe$, when Ca/Fe exceeds 0.1 (Fig. 3; Table 5). However, for

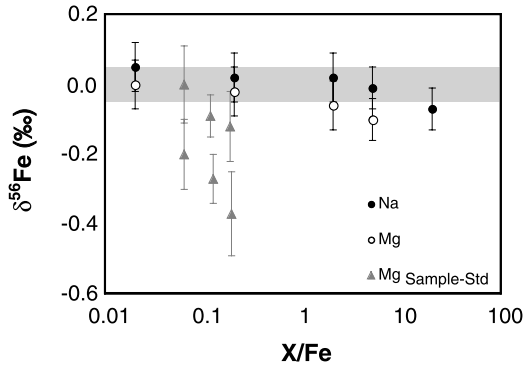

Fig. 2. DS-corrected Fe isotope ratios for IRMM-14 standards doped with Na and Mg obtained during two analytical sessions. The shaded area marks the range of results for pure IRMM-14 standards during the two sessions, whereas the error bars show the internal precision of the individual analyses (2 SE). The grey triangles represent Fe isotope ratios determined for Mg-doped samples analysed using the standard-sample bracketing method (Albarède and Beard, 2004).

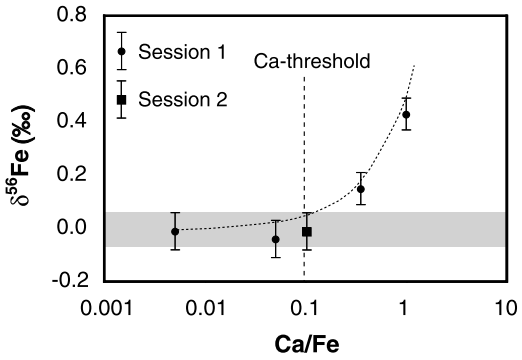

Fig. 3. DS-corrected Fe isotope ratios for IRMM-14 standards doped with Ca obtained during two analytical sessions. The shaded area indicates the range of results for pure IRMM-14 standards during each session, whereas the error bars show the internal precision of the individual analyses (2 SE). Isobaric interferences of CaN^+, CaO^+, and $CaOH^+$ generate erroneous DS-corrected $\delta^{56}Fe$ at $Ca/Fe > 0.1$. The dotted line represents the theoretical departure of $\delta^{56}Fe$ from the IRMM-14 composition based on the CaN^+, CaO^+, and $CaOH^+$ production estimated from measurements on a pure Ca solution. Based on these results, we interpret that samples with $Ca/Fe \leqslant 0.1$ yield reliable DS-corrected Fe isotope ratios (marked as Ca-threshold in the figure).

samples with $Ca/Fe \leqslant 0.1$ the analytical results obtained during two sessions were not appreciably affected by isobaric interferences and matrix-induced changes in instrumental mass bias. Fig. 3 also shows *calculated* $\delta^{56}Fe$ values resulting from Ca-based interferences on IRMM-14. The estimates of the production of polyatomic Ca interference on masses 54, 56, 57, and 58 were based on the signals observed on 54, 56, 57, and 58 while aspirating a pure Ca solution (25 ppm). These calculations are in agreement with the results for the analysed samples. As proposed by Kehm et al. (2003), the use of conventional plasma efficiency leads to markedly lower CaO^+ and $CaOH^+$ production. Based on our results, we calculate a $^{40}CaO^+/Ca^+$ production factor of <1‰ for our instrument and an even smaller production of $^{40}CaOH^+$.

To further evaluate the veracity of our method, pure and chemically doped IRMM-14 samples were passed through the anion exchange separation procedure. For the solutions derived from very low-Fe calcite, three passes through the exchange columns were sometimes necessary to obtain satisfactory results. To test the effect of the three passes, we used an aliquot of IRMM-14 and followed the same procedure. The measured Fe isotope composition (Table 6) was identical to that of the mean IRMM-14 data. Further experiments showed that a synthetic mixture of Fe with Cr and Ni in equal concentrations yields accurate DS-corrected Fe isotope ratios after only one column pass. A synthetic mixture of IRMM-14 and solution from pure calcite with a starting $Ca/Fe = 1000$ (equivalent to a Fe concentration of ca. 400 ppm in calcite) also yielded accurate Fe isotope data after three column passes.

To probe if incomplete dissolution caused isotope fractionation during sample processing, additional material from SLS-10, the sample that had the most residual solid after HCl digestion, was digested with HF and passed through the columns. The analysed Fe isotope composition did not differ significantly from that obtained for the HCl digestion.

Table 6
DS-corrected Fe isotope ratios of treated and untreated IRMM-14 standards and limestone SLS-10 after anion exchange separation

Sample	Type	Column passes	$\delta^{56}Fe$ (‰)	2 SE
IRMM-14	Only standard	3	−0.03	0.06
	+ equal Ni and Cr	1	0.05	0.09
	+ $CaCO_3$, $Ca/Fe = 1000$	3	−0.02	0.05
	+ citrate, $Cit/Fe = 20{,}000$	1	−0.04	0.05
SLS-10 limestone	HF digest	3	−0.29	0.06
	HCl digest	3	−0.25	0.06
	HCl digest—prespiked	3	−0.17	0.08
		3	−0.12	0.06

For IRMM-14 standards, the treatment included doping with Ni and Cr, calcite or citrate before separation, For the organic-containing SLS-10, the treatment consisted of spiking prior to separation.

Finally, experiments were performed to examine whether dissolved organic ligands compete with chloride during Fe-complex formation. The presence of organically bonded Fe, which may have a low affinity for adsorption to the resin, could lead to Fe leaching during elution. In this experiment, citrate was added to the IRMM-14 solution prior to anion exchange chemistry. Citrate has several properties that could compromise Fe separation. It complexes with Fe in acidic solutions (shown by calculations with PHREEQC, Parkhurst and Appelo, 1999, using the MINTEQ database of Allison et al., 1990) and it may also act as a reducing agent for Fe(III) (Gutteridge, 1991). However, in the presence of citrate, we observed no breakthrough of Fe from the column in 6 M HCl and the analysed Fe was isotopically identical to the mean value obtained for IRMM-14 (Table 6). Similarly, the isotope composition of collected Fe showed only very slight variation when the limestone sample SLS-10 that contained dissolved organic compounds was spiked before Fe separation, or when the sample was treated using our normal procedures. This suggests that the presence of organic ligands compromises Fe treatment by the columns to an extent that is barely resolvable.

4.3. Fe isotope composition of standard reference materials

DS-corrected Fe isotope data for 15 standard reference materials are presented in Fig. 4 and Table 7. Apart from the ferromanganese nodules, the standards show very similar Fe isotope compositions. Eight igneous rocks have a mean $\delta^{56}Fe$ of 0.041 ± 0.11‰ which is consistent with averages reported for similar material by Poitrasson et al. (2004) (0.068 ± 0.08‰; $n = 13$) and Beard et al. (2003a) ($\delta^{56}Fe = 0.09 \pm 0.10$‰; $n = 46$). Fig. 4 also shows the Fe isotope composition of some of these standard reference materials that have been analysed in other laboratories. Generally, there is good agreement between the results of

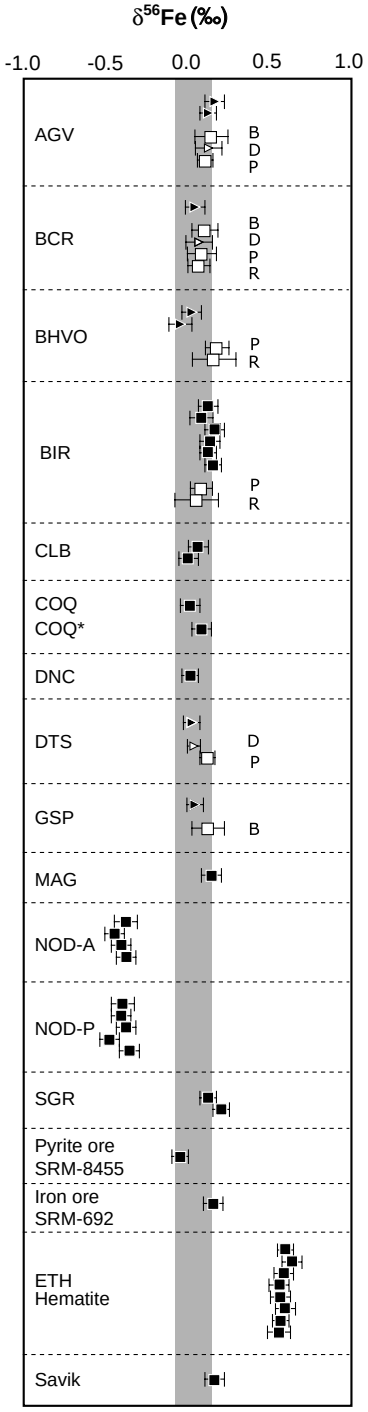

Fig. 4. Fe isotope compositions of standard reference materials obtained in this and previous studies. The filled symbols represent DS-corrected Fe isotope ratios determined in this study. For these samples, the error bars reflect the internal precision of the analyses (2 SE). The open symbols refer to results of other studies: B, Beard et al. (2003a); D, Dauphas et al. (2004); P, Poitrasson et al. (2004); R, Rouxel et al. (2003). These data have all been normalised to IRMM-14 and error bars represent 2 SD for samples analysed > 3 times and reported external reproducibility for samples analysed < 3 times. The square symbols represent first-generation standards (e.g., AGV-1), whereas triangle symbols represent the second-generation standards (e.g., AGV-2). The shaded area refers to the bulk Earth value determined by Beard et al. (2003a). In general, our results are in excellent agreement with those reported in previous studies.

Table 7
DS-corrected Fe isotope data for standard reference materials

Sample name	δ^{56}Fe (‰)	2 SE	Average	2 SD
AGV-2	0.15	0.06	0.13	—
	0.11	0.05		
BCR-2	0.03	0.06		
BHVO-2	0.01	0.06	−0.03	—
	−0.06	0.07		
BIR-1	0.11	0.06	0.12	0.06
	0.07	0.07		
	0.15	0.06		
	0.12	0.06		
	0.11	0.05		
	0.14	0.05		
CLB-1	0.05	0.06	0.02	—
	−0.01	0.06		
COQ-1	0.00	0.06		
	0.07[a]	0.06		
DNC-1	0.00	0.05		
DTS-2	0.01	0.05		
GSP-2	0.03	0.05		
MAG-1	0.13	0.06		
NOD-A-1	−0.39	0.07	−0.42	0.07
	−0.46	0.06		
	−0.42	0.06		
	−0.39	0.06		
NOD-P-1	−0.41	0.07	−0.42	0.09
	−0.42	0.06		
	−0.39	0.06		
	−0.49	0.06		
	−0.37	0.06		
SGR-1	0.11	0.05	0.15	—
	0.19	0.05		
SRM-8455	−0.06	0.05		
SRM-692	0.14	0.06		
ETH hematite	0.58	0.05	0.58	0.05
	0.62	0.06		
	0.57	0.06		
	0.54	0.06		
	0.55	0.06		
	0.58	0.06		
	0.55	0.05		
	0.54	0.07		
Iron meteorite—Cape York	0.15	0.06		

[a] Spiked before chemical purification.

this and previous studies. The iron meteorite, sedimentary standards, pyrite ore, and iron ore do not deviate from the mean value for igneous rock standards by more than 0.11‰. The two ferromanganese nodule samples are both isotopically light and yield identical $\delta^{56}Fe = -0.42$‰, a value that falls in the middle of the range of the isotopically light Fe values ($\delta^{56}Fe = -0.8$ to 0.0‰.) recently reported for hydrogenetic ferromanganese deposits from the world's oceans (Levasseur et al., 2004).

Table 8
DS-corrected Fe isotope data for calcium carbonate samples

Environment	Sample	δ^{56}Fe (‰)	2 SE
Magmatic	MAG BB 10	−0.01	0.06
Skarn	S-89a	−0.07	0.06
Marble	LS 9	−0.45	0.06
Limestone	SLS 08 *Steinvika*	−0.21	0.06
	SLS 10 *Steinvika*	−0.25	0.06
	L BB3	−0.95	0.07
Hydrothermal	HTC 4 *Steinvika*	−0.27	0.05
	HTC 12 *Steinvika*	−0.73	0.05
	HTC 28 *Steinvika*	−1.25	0.06
	HTC 38 *Steinvika*	−0.69	0.05
		−0.66	0.06
	HTC 40 *Steinvika*	−0.89	0.06
		−0.82	0.07
		−0.83	0.06
	HT/RM 326	−0.38	0.06
	HT 9572	−1.20	0.06
	HT 9426	−0.39	0.06
Pegmatite	P 31867	−1.20	0.05
		−1.17	0.06
	P9710	−0.29	0.06
Slickenslide	Slick 1	−0.27	0.06

4.4. Fe isotope composition of natural calcium carbonate materials

The calcium carbonate samples have δ^{56}Fe ranging from 0.0 to −1.3‰ (Table 8) and, apart from the magmatic carbonate (carbonatite), are all lighter than the bulk Earth value determined by Beard et al. (2003a). These results indicate that significant fractionation of Fe isotopes occurs at relatively high temperatures given the conditions under which some of these carbonate minerals formed.

The magmatic and skarn carbonate samples have δ^{56}Fe ≈ 0‰ (Fig. 5), consistent with those of other analyses of igneous crustal material (Beard et al., 2003a), whereas the marble and slickenslide samples display somewhat lighter Fe isotope compositions. Pegmatite and hydrothermal calcite display a greater range of compositions ranging from δ^{56}Fe ≈ −0.3 to −1.3‰. It is notable that Fe incorporated in the hydrothermal calcite samples of the Steinvika Formation, which were sampled within a relatively restricted volume of ca. $500 \times 500 \times 100$ m^3, display a large variation in Fe isotope composition. Their Fe isotope values are generally lighter than those of the host limestone (Fig. 5; Table 8).

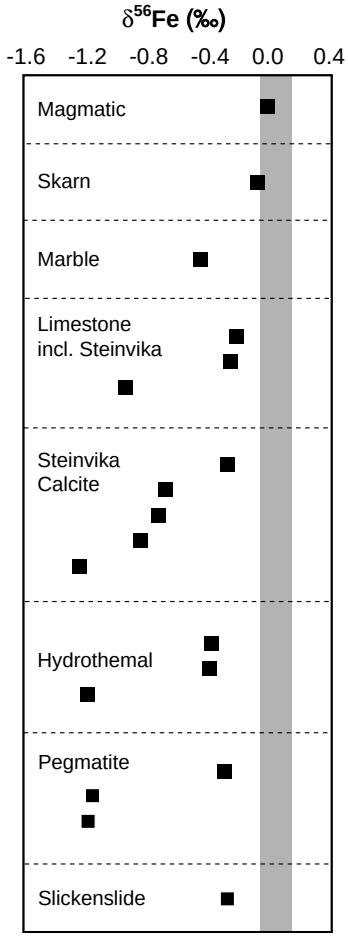

Fig. 5. DS-corrected Fe isotope ratios for natural calcium carbonate samples. All the non-magmatic samples have Fe isotope compositions lighter than the average bulk Earth (shaded area; Beard et al., 2003a).

5. Discussion

5.1. Double spike method for Fe isotope analysis by MC-ICP-MS

DS-corrected Fe isotope data for the ETH in-house standard are reproducible to ±0.05‰ (2 SD) on δ^{56}Fe with a single analysis and data for standard reference materials are in agreement with other studies. The most likely explanation for the small session-to-session "jumps" in mean values observed for IRMM-14 is that they reflect slight changes in production of Fe hydride interferences, which affect the ^{57}Fe/^{56}Fe ratio. Earlier studies have identified that ^{56}FeH$^+$/^{56}Fe production amounts to approximately 5 ppm (Arnold et al., 2004). Using this value, the contribution of ^{56}FeH$^+$ on the ^{57}Fe signal translates into a 0.5‰ contribution after data reduction. Thus, session-to-session changes in ^{56}FeH$^+$/^{56}Fe production may contribute to the session-to-session difference observed in our standard values. However, these can be readily corrected for, provided 4–5 standards are analysed during each session. Our reproducibility is comparable to those obtained by other MC-ICP-MS methods and indicates that the DS-method with MC-ICP-MS is an effective way of quickly generating precise and accurate Fe isotope data. Also, it is less susceptible to matrix effects than sample-standard bracketing methods (Figs. 2 and 3).

The major limiting constraint on DS data quality is the uncertainty of the ^{57}Fe/^{56}Fe ratio, which is influenced by both the statistics of measuring the small ^{57}Fe ion beam and the subtraction of the very small and difficult to measure mass 57 background resulting from Ar-based isobaric

interferences. Further development of MC-ICP-MS instruments should enable DS-corrected Fe isotope data to be produced that represent a significant improvement over our study. A high-resolution instrument equipped with Faraday collectors with a greater dynamic range, enabling measurement of a larger 57 signal, could have the potential to resolve very small isotopic differences as low as 0.01‰.

It should be noted that the DS-method does not allow identification of isotope compositions that differ from those predicted by the terrestrial mass-dependent fractionation curve without analysis of an unspiked sample. For example, meteorite samples could have Fe isotope signatures that are influenced by nucleosynthetic processes. Another potential problem for the DS method might arise from the very subtle differences in mass-dependent fractionation curves for kinetic or equilibrium isotope effects, such as those reported for Mg isotopes (Young et al., 2002). In the case of Fe, however, fractionation curves representing kinetic and equilibrium isotope effects are barely resolvable because the Fe isotope fractionation in nature is very small (Malinovsky et al., 2003). For example, even for highly fractionated samples, such as the haemoglobin analysed by Zhu et al. (2002), which has $\delta^{57}Fe \approx -5‰$, the expected $\delta^{56}Fe$ for kinetic and equilibrium isotope effects are −3.36 and −3.39‰, respectively, based on the calculations of Malinovsky et al. (2003). This 0.03‰ difference in $\delta^{56}Fe$ would not introduce significant errors during DS-data reduction.

5.2. Fe isotope variations in natural calcium carbonate samples

Fe isotope compositions measured for calcium carbonate samples range from $\delta^{56}Fe = 0.0$ to −1.3‰ The lightest Fe isotope compositions were determined for pegmatitic material and hydrothermal calcites. For the pegmatitic sample, it seems unlikely that the very negative $\delta^{56}Fe$ represents only equilibrium fractionation between aqueous Fe(II) and structural Fe in the carbonates, considering the high temperature (>500 °C) at which formation is likely to have occurred. It is more feasible that the observed Fe isotope ratios are inherited from a fluid with isotopically light Fe. Pegmatite formation represents the final, fluid-rich stage of igneous activity and the progressive formation of Fe-bearing minerals during magma differentiation may have, through a Rayleigh-type fractionation process, lead to isotopically light residual Fe in the final fluid.

The calcite samples from the Steinvika Formation provide a useful setting for investigating the processes that could affect Fe isotope fractionation in hydrothermal systems. These samples include both euhedral calcite crystals that have grown in a vein and the matrix limestone source material. The samples were taken from within a relatively small volume, and the mineral assemblage and morphology of the calcite crystals suggest similar overall formation conditions, i.e., hydrothermal recrystallisation at temperatures of 250–400 °C (Harstad, pers. commun.). Even given the relatively limited variation in physical conditions of recrystallisation, the analysed samples display significant variation in Fe isotope composition ($\delta^{56}Fe = -0.3$ to −1.3‰).

For one of the hydrothermally precipitated calcite crystals, analysis of a goethite-rich part yielded $\delta^{56}Fe = -0.68‰$, whereas a $\delta^{56}Fe$ value of −0.85‰ was determined for a region where Fe(II) was exclusively incorporated in the calcite structure. Based on the relatively high formation temperature and the well-developed calcite morphology, which suggests slow precipitation, the small, but significant, $\Delta^{56}Fe_{goethite-calcite} = 0.17 \pm 0.10$ (2 SD) may reflect processes occurring while co-existing phases were at equilibrium.

Equilibrium isotope fractionation can be described as a function of temperature, as a result of changes in the vibrational frequencies of bonds (Urey, 1947). When modelling this behaviour, studies often employ reduced partition function ratios, which express the equilibrium isotope ratio for a given substance relative to the isotope ratio of the dissociated atoms (Schauble et al., 2001). For two substances, the combination of their reduced partition function ratios yields the equilibrium fractionation factor. The combination of the reduced partition functions is often expressed in units that adequately approximate the equilibrium isotope fractionation expressed in the δ notation (Schauble et al., 2001), i.e., one unit of 1000 $\ln\alpha \sim 1‰$ fractionation. For Fe isotopes, reduced partition function ratios have been estimated from Mössbauer and vibrational spectroscopy data for a range of Fe-bearing compounds and complexes (Polyakov and Mineev, 2000; Schauble et al., 2001). In general, the data predict that the magnitude of isotopic fractionation decreases with increasing temperature and that strong bonding of Fe favours incorporation of heavy isotopes, meaning that Fe(II)-bearing compounds tend to be isotopically light compared to the more covalently bonded Fe(III)-bearing compounds. Unfortunately, reduced partition function ratios for trace Fe(II) incorporated in the calcite structure have not been determined, so reduced partition function ratios for siderite are used here as an approximate model.

For equilibrium fractionation between siderite and goethite, Mössbauer spectroscopy data predict that the observed $\Delta^{56}Fe_{goethite-calcite}$ is associated with a temperature of ca. 675 °C (including uncertainties in the Fe isotope measurement, the data predict a temperature of above ca. 490 °C). This formation temperature is inconsistent with observed mineral assemblages (Harstad, pers. commun.), corroborating suggestions that Mössbauer spectroscopy data overestimate isotope fractionation (Johnson et al., 2003).

The qualitative implications of reduced partition function ratios are, however, generally consistent with observed Fe isotope variation in nature and in the laboratory (Beard and Johnson, 2003; Johnson et al., 2002, 2003). The ratios, combined and extrapolated from Mössbauer and vibrational spectroscopy data, may aid in the understanding of Fe isotope behaviour. Fig. 6 shows that

little fractionation occurs when siderite and goethite precipitate from a solution where Fe speciation is dominated by $Fe(II)_{(aq)}$. On the other hand, both spectroscopic and experimental data suggest that significant fractionation occurs between Fe(II)– and Fe(III)–aquo complexes. Also, given that the magnitude of Fe isotope fractionation between Fe(II)– and Fe(III)–aquo complexes is governed primarily by Fe–O bonding, which depends mostly on the Fe redox state, the presence of Fe–hydroxyl complexes is expected to be of minor importance (Johnson et al., 2002). Thus, siderite and goethite may incorporate light Fe isotopes during precipitation from a solution where Fe speciation is dominated by Fe(III)–aquo or –hydroxyl complexes or other Fe complexes having higher bond-strength.

For the samples of the Steinvika Formation, the negative, but similar, δ^{56}Fe values for the goethite and calcite samples hint at the mechanisms that may have controlled the Fe isotope composition of the hydrothermal system:

1. Assuming that the Fe speciation of the hydrothermal solution consisted dominantly of Fe(II)–aquo and –hydroxyl complexes, the fluids from which the goethite and calcite precipitated may have been largely light in Fe isotopes. The goethite and calcite isotope composition may, therefore, reflect the solution signature. The Fe isotope composition of the hydrothermal solution could reflect input of light isotopes from hydrothermal fluids from the intrusive body. High-precision analyses of hydrothermal fluids from mid-ocean ridges have shown that dissolved Fe is only slightly light when emerging from vents ($\delta^{56}Fe \approx -0.2$; Beard et al., 2003b; Severmann et al., 2004). These fluids, however, stem from basaltic magmatic activity. Fluids that originate from evolved, felsic magmatic bodies may have a different Fe isotope signature. Alternatively, the isotope composition of the solution from which the calcite precipitated may reflect local processes. In this scenario, the Fe isotope composition of the solution could be attributable to precipitation in the hydrothermal fractures of phases that favour incorporation of heavier isotopes (Fig. 7A), e.g., some iron oxides (Polyakov and Mineev, 2000). Alternatively, dissolution of Fe-bearing silicates in the limestone may have preferentially released isotopically light Fe, in a fashion similar to that observed for hydrothermal leaching during ocean crust alteration (Rouxel et al., 2003) or for ligand-induced dissolution of hornblende (Brantley et al., 2004). The wide range of δ^{56}Fe determined for the calcites may indicate that the dissolving Fe changes isotope composition, possibly because the Fe residue in the dissolving silicates becomes increasingly heavy during leaching of light isotopes leading to Rayleigh-type fractionation (Fig. 7B).
2. The observed δ^{56}Fe values are also consistent with a solution having an Fe isotope composition of more bulk Earth like values, provided that the solutions contain appreciable amounts of aqueous Fe species, with significantly larger reduced partition function ratios than $Fe(II)(H_2O)_6^{2+}$. Such species could include Fe(III)–aquo and –hydroxyl complexes (Fig. 7C) or Fe(II) complexes with organic ligands, which may form strong bonds and lead to fractionation of Fe isotopes in the aqueous phase. Presence of aqueous Fe(III) species is consistent with the precipitation of Fe(III)–hydroxides, such as goethite. However, synthesis experiments performed at temperatures lower than those presumed to have prevailed during the formation of our samples have shown that Fe(III) strongly inhibits the growth of calcite crystals (Dromgoole and Walter, 1990). Thus, high concentrations of aqueous Fe(III) may be inconsistent with the formation of morphologically well-developed calcite crystals.

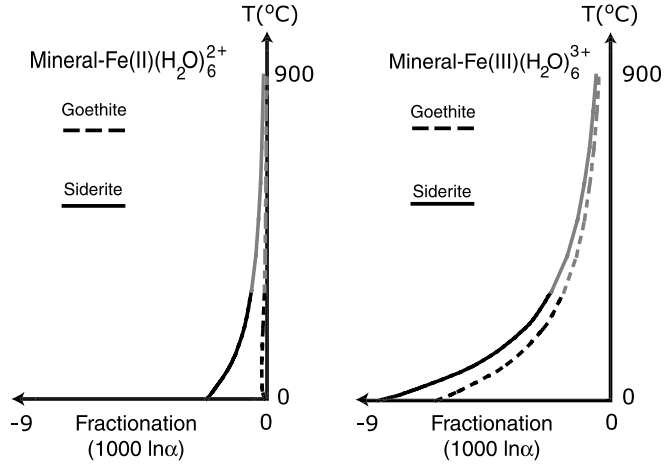

Fig. 6. Fe isotope fractionation during formation of siderite and goethite in isotopic equilibrium with $Fe(II)(H_2O)_6^{2+}$ or $Fe(III)(H_2O)_6^{3+}$. The isotope composition of Fe incorporated in the two phases is considerably lighter when the aqueous Fe is trivalent. One unit of 1000 $\ln\alpha \sim 1‰$ fractionation. The figure is based on a combination of the data from Polyakov and Mineev (2000) and Schauble et al. (2001). Reduced partition function ratios for aqueous Fe complexes only cover the range of 0–300 °C (Schauble et al., 2001). The grey part of the curves represents data that have been extrapolated under the assumption that the fractionation between mineral phases and aqueous phases displays a temperature dependency similar to that predicted for siderite–goethite fractionation.

In summary, calcite predominantly incorporates Fe(II) during precipitation. The data suggest that Fe incorporated into Ca sites in the structure largely reflects the isotope composition of the $Fe(II)_{(aq)}$ pool of the solution, and that this pool of Fe may have been affected by a variety of isotope fractionation mechanisms during its pathway into the solution.

6. Conclusions

The use of a ^{58}Fe–^{54}Fe DS enables rapid determination of Fe isotope composition by MC-ICP-MS to a precision of ±0.05‰ (2 SD). This method is relatively insensitive to the presence of non-isobaric matrix elements compared

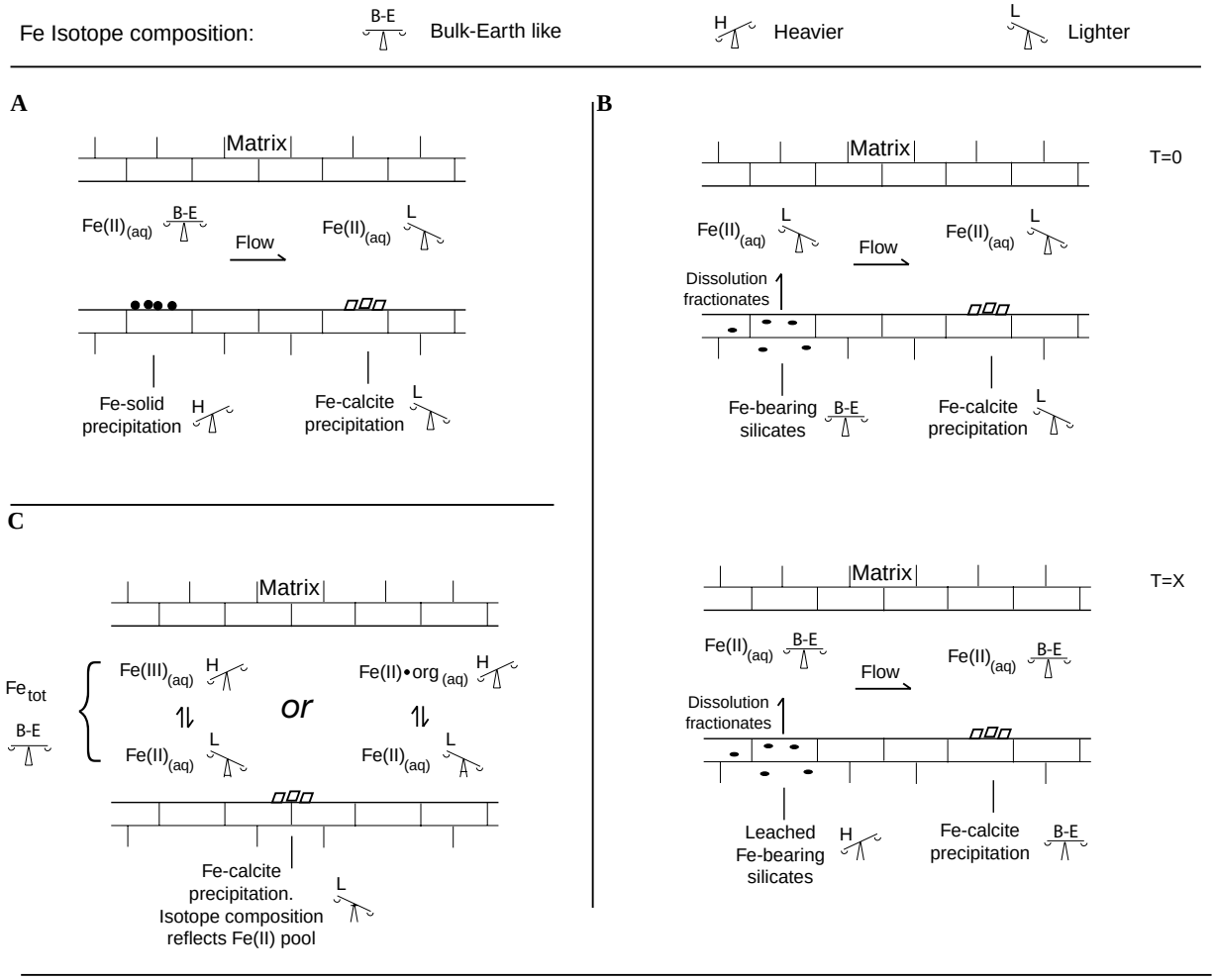

Fig. 7. (A) Precipitation of Fe-bearing phases incorporating heavier isotopes leads to lighter residual Fe in the solution. The isotope composition of the precipitating Fe-calcite reflects solution composition. (B) Dissolution of Fe-bearing silicates with Bulk-Earth like Fe isotope composition in the limestone leads to selective leaching of lighter isotopes. The preferential leaching leads to a heavy residue in the silicates and further dissolution would release heavier Fe isotopes, possibly approaching Bulk-Earth like composition. The isotope composition of the precipitating Fe-calcites reflects the solution composition. (C) Spectroscopic data predict that strongly bonded Fe atoms will tend to have a heavier isotope composition than more weakly bonded Fe atoms (Fig. 6). The presence of significant amounts of strongly bonded aqueous Fe species may thus give rise to significant isotope fractionation between aqueous Fe species. Preferential precipitation of light Fe species (e.g., Fe(II)) could then lead to the formation of Fe-calcites with light Fe isotope compositions from an aqueous reservoir of bulk-Earth like composition. Based on the theoretical data, Fe(III) and Fe(II) organic complexes are likely to be more strongly bonded than $Fe(II)_{(aq)}$ species.

to the sample-standard bracketing method. Analyses of IRMM-14 standards doped with Na and Mg show that double spiking corrects effectively for instrumental mass-bias, even when the concentrations of these elements exceed that of Fe.

DS-corrected Fe isotope data for several international standard reference materials and calcium carbonate from a range of geological environments have been collected. The igneous standard reference materials have Fe isotope ratios comparable with those of other recent studies. Fe isotope data for hydrothermal and metamorphic calcium carbonate rocks display significant variation, and the Fe is predominantly lighter than the bulk Earth ($\delta^{56}Fe = -0.07$ to $-1.25‰$), showing that significant isotopic fractionation may occur at relatively high temperatures where bacterial activity is unlikely.

The Fe isotope composition of structural Fe in hydrothermal calcites was also analysed and varies from $\delta^{56}Fe = -0.27$ to $-1.25‰$. The observed variation may reflect the composition of the hydrothermal solution, which may, in turn, be governed by selective leaching of light Fe from silicates in the limestone matrix or by magmatic processes in the nearby intrusion. Alternatively, the presence of Fe(III) or organic material in the hydrothermal fluid during calcite precipitation may lead to the observed light Fe isotope composition.

Acknowledgments

We thank Andreas Harsted, Jane Christensen, Bjørn Buchardt, and Lars Stemmerik for providing some of the sample materials and discussions about this work. Martin

Bizzarro contributed to numerous stimulating discussions on Fe isotope analysis. Helen Williams kindly provided us with some of the ETH hematite standard and assisted in the preparation of the DS. We are grateful for the encouragement of Eva-Lena Tullborg, John Smellie, and Ignasi Puigdomenech. We also thank Steen Mørup and Cathrine Frandsen for conducting the Mössbauer spectroscopy. Finally, we acknowledge Joseph Skulan and two anonymous reviewers for their very constructive and helpful comments.

Associate editor: James Farquhar

References

Albarède, F., Beard, B.L., 2004. Analytical methods for nontraditional stable isotopes. *Rev. Mineral. Geochem.* **55**, 113–152.

Allison, J.D., Brown, D.S., Novo-Gradac, K.J., 1990. *MINTEQA2/PRODEFA2—A Geochemical Assessment Model for Environmental Systems: Version 3.0 User's Manual*. U.S. Environmental Protection Agency. Athens, Georgia.

Anbar, A.D., Roe, J.E., Barling, J., Nealson, K.H., 2000. Nonbiological fractionation of iron isotopes. *Science* **288**, 126–128.

Arnold, G.L., Weyer, S., Anbar, A.D., 2004. Fe isotope variations in natural materials measured using high mass resolution multiple collector ICPMS. *Anal. Chem.* **76**, 322–327.

Beard, B.L., Johnson, C.M., 1999. High precision iron isotope measurement of terrestrial and lunar materials. *Geochim. Cosmochim. Acta* **63**, 1653–1660.

Beard, B.L., Johnson, C.M., 2003. High and low temperature applications of Fe isotope geochemistry. *Geochem. News* **117**, 8–13.

Beard, B.L., Johnson, C.M., Cox, L., Sun, H., Nealson, K.H., Aguilar, C., 1999. Iron isotope biosignature. *Science* **285**, 1889–1892.

Beard, B.L., Johnson, C.M., Skulan, J.L., Nealson, K.H., Cox, L., Sun, H., 2003a. Application of Fe isotopes to tracing the geochemical and biological cycling of Fe. *Chem. Geol.* **195**, 87–117.

Beard, B.L., Johnson, C.M., Von Damm, K.L., Poulson, R.L., 2003b. Isotope constraints on Fe cycling and mass balance in oxygenated earth oceans. *Geology* **31**, 629–632.

Brantley, S.L., Liermann, L.J., Guynn, R.L., Anbar, A., Icopini, G.A., Barling, J., 2004. Fe isotopic fractionation during mineral dissolution with and without bacteria. *Geochim. Cosmochim. Acta* **68**, 3189–3204.

Bullen, T.D., White, A.F., Childs, C.W., Vivit, D.V., Schulz, M.S., 2001. Demonstration of significant abiotic iron isotope fractionation in nature. *Geology* **29**, 699–702.

Dauphas, N., Janney, P.E., Mendybaev, P.A., Wadhwa, M., Richter, F.M., Davis, A.M., van Zuilen, M., Hines, R., Foley, C.N., 2004. Chromatographic separation and MC-ICPMS analysis of iron, investigating mass dependent and independent isotope effects. *Anal. Chem.* **76**, 5855–5863.

Douglas, D.J., Tanner, S.D., 1998. Fundamental considerations in ICPMS. In: Montaser, A. (Ed.), *Inductively Coupled Plasma Mass Spectrometry*. Wiley VCH, New York, pp. 615–679.

Dromgoole, E.L., Walter, L.M., 1990. Iron and manganese incorporation into calcite: effects of growth kinetics, temperature and solution chemistry. *Chem. Geol.* **81**, 311–336.

Eugster, O., Tera, F., Wasserburg, G.J., 1969. Isotopic analysis of barium in meteorites and in terrestrial samples. *J. Geophys. Res.* **74**, 3897–3908.

Gutteridge, J.M.C., 1991. Hydroxyl radical formation from the autoreduction of a ferric citrate complex. *Free Radic. Bio. Med.* **11**, 401–406.

Hofmann, A., 1971. Fractionation correction for mixed-isotope spikes of Sr, K and Pb. *Earth Planet. Sci. Lett.* **10**, 397–402.

Ingle, C.P., Sharp, B.L., Horstwood, M.S.A., Parrish, R.R., Lewis, D.J., 2003. Instrument response functions, mass bias and matrix effects in isotope ratio measurement and semi-quantitative analysis by single and multi-collector ICP-MS. *J. Anal. At. Spectrom.* **18**, 219–229.

Johnson, C.M., Beard, B.L., 1999. Correction of instrumentally produced mass fractionation during isotopic analysis of Fe by thermal ionization mass spectrometry. *Int. J. Mass Spectrom.* **193**, 87–99.

Johnson, C.M., Skulan, J.L., Beard, B.L., Sun, H., Nealson, K.H., Braterman, P.S., 2002. Isotopic fractionation between Fe(III) and Fe(II) in aqueous solutions. *Earth Planet. Sci. Lett.* **195**, 141–153.

Johnson, C.M., Beard, B.L., Beukes, N.J., Klein, C., O'Leary, J.M., 2003. Ancient geochemical cycling in the Earth as inferred from Fe isotope studies of banded iron formations from the Transvaal Craton. *Contrib. Mineral. Petrol.* **144**, 523–547.

Kehm, K., Hauri, E.H., Alexander, C.M.O., Carlson, R.W., 2003. High precision iron isotope measurement of meteoritic material by cold plasma ICP-MS. *Geochim. Cosmochim. Acta* **67**, 2879–2891.

Levasseur, S., Frank, M., Hein, J.R., Halliday, A.N., 2004. The global variation in the iron isotope composition of marine hydrogenetic ferromanganese deposits: implications for seawater chemistry. *Earth Planet. Sci. Lett.* **224**, 91–105.

Malinovsky, D., Stenberg, A., Rodushkin, I., Andren, H., Ingri, J., Öhlander, B., Baxter, D.C., 2003. Performance of high resolution MC-ICP-MS for Fe isotope ratio measurements in sedimentary geological materials. *J. Anal. At. Spectrom.* **18**, 687–695.

Maréchal, C.N., Télouk, P., Albarède, F., 1999. Precise analysis of copper and zinc isotopic compositions by plasma-source mass spectrometry. *Chem. Geol.* **156**, 251–273.

Matthews, A., Morgan-Bell, H.S., Emmanuel, S., Jenkyns, H.C., Erel, Y., Halicz, L., 2004. Controls on iron-isotope fractionation in organic-rich sediments (Kimmeridge Clay, Upper Jurassic, southern England). *Geochim. Cosmochim. Acta* **68**, 3107–3123.

Parkhurst, D.L., Appelo, C.A.J., 1999. *User's guide to PHREEQC (version 2)—A Computer Program for Speciation, Batch-Reaction, One-dimensional Transport, and Inverse Geochemical Calculations*. Water-Resources Investigations Report 99-4259. U.S. Geological Survey, Denver.

Poitrasson, P., Halliday, A.N., Lee, D.-C., Levasseur, S., Teutsch, N., 2004. Iron isotope difference between Earth, Moon, Mars and Vesta as possible records of contrasted accretion mechanisms. *Earth Planet. Sci. Lett.* **223**, 253–266.

Polyakov, V., Mineev, S., 2000. The use of Mössbauer spectroscopy in stable isotope geochemistry. *Geochim. Cosmochim. Acta* **64**, 849–865.

Roe, J.E., Anbar, A.D., Barling, J., 2003. Non-biological fractionation of Fe isotopes: evidence of an equilibrium isotope effect. *Chem. Geol.* **195**, 69–85.

Rouxel, O., Dobbek, N., Ludden, J., Fouquet, Y., 2003. Iron isotope fractionation during oceanic crust alteration. *Chem. Geol.* **202**, 155–182.

Schauble, E.A., Rossman, G.R., Taylor Jr., H.P., 2001. Theoretical estimates of equilibrium Fe-isotope fractionation from vibrational spectroscopy. *Geochim. Cosmochim. Acta* **65**, 2487–2497.

Severmann, S., Johnson, C.M., Beard, B.L., German, C.R., Edmonds, H.N., Chiba, H., Green, D.R.H., 2004. The effect of plume processes on the Fe isotope composition of hydrothermally derived Fe in the deep ocean as inferred from the Rainbow vent site, Mid-Atlantic Ridge, 36 degrees 14′N. *Earth Planet. Sci. Lett.* **225**, 63–76.

Sharma, M., Polizzotto, M., Anbar, A.D., 2001. Iron isotopes in hot springs along the Juan de Fuca Ridge. *Earth Planet. Sci. Lett.* **194**, 39–51.

Siebert, C., Nägler, T.F., Kramers, J.D., 2001. Determination of molybdenum isotope fractionation by double-spike multicollector inductively coupled plasma mass spectrometry. *Geochem. Geophys. Geosys.*, **2**, Art. No. 2000GC000124.

Urey, H.C., 1947. The thermodynamic properties of isotopic substances. *J. Chem. Soc. Lond.*, 562–581.

Walczyk, T., von Blanckenburg, F., 2002. Natural iron isotope variation in human blood. *Science* **295**, 2065–2066.

Williams, H.M., McCammon, C.A., Peslier, A.H., Halliday, A.N., Teutsch, N., Levasseur, S., Burg, J.-P., 2004. Iron isotope fractionation and the oxygen fugacity of the mantle. *Science* **304**, 1656–1659.

Young, E.D., Galy, A., Nagahara, H., 2002. Kinetic and equilibrium mass-dependent isotope fractionation laws in nature and their geochemical and cosmochemical significance. *Geochim. Cosmochim. Acta* **66**, 1095–1104.

Zhu, X.K., O'Nions, R.K., Guo, Y., Reynolds, B.C., 2000. Secular variation of iron isotopes in North Atlantic Deep Waters. *Science* **287**, 2000–2002.

Zhu, X.K., Guo, Y., Williams, R.P.J., O'Nions, R.K., Matthews, A., Belshaw, N.S., Canters, G.W., de Waal, E.C., Weser, U., Burgess, B.K., Salvato, B., 2002. Mass fractionation processes of transition metal isotopes. *Earth Planet. Sci. Lett.* **200**, 47–62.